



A Rudimentary Computational Assessment of Low Tip Speed Ratio Asymmetrical Wind Turbine Blades

S.N. Ashwindran¹, A.A. Azizuddin^{1*}, A.N. Oumer¹

¹Faculty of Mechanical and Automotive Engineering Technology,
Universiti Malaysia Pahang, Pekan, 26600, MALAYSIA

*Corresponding author

DOI: <https://doi.org/10.30880/ijie.2020.12.04.010>

Received 8 May 2019; Accepted 27 December 2019; Available online 30 April 2020

Abstract: This paper presents a computational study of novel drag type vertical axis wind turbine inspired by three design elements from nature. The aim of this study is to analyze the aerodynamic performance of the proposed design. The design is simulated in FLUENT using *SST k- ω* transport model via URANS turbulent model. The model is simulated in 2D in order to save computational time. The design is simulated under the influence of freestream velocity of $U_{\infty}=8\text{m/s}$ at multiple tip speed ratios. The proposed wind turbine is composed of drag induced novel cavity vane turbine blade for energy capturing. The proposed wind turbine generated low power coefficient, $C_p = 0.029$ and $C_p=0.025$ at $\lambda=0.2$ and $\lambda=0.3$ respectively. Tip speed ratio $\lambda=0.4$, $\lambda=0.6$ and $\lambda=0.9$ indicated high instability in moment generation and high negative power extraction. Computational result indicated that the geometry of the cavity vane has impacted the performance of the turbine due to its sharp-edged corner. The proposed geometry resulted in unstable moment generation and torque deliverance which impacted the power extraction. The lack of symmetrical and streamline properties of the blades has affected one another as in terms of rotation. The cavity vane experiences high adverse pressure due to its sharp cornered geometry in returning blade which consequently impacted the rotation of the advancing blade.

Keywords: Vertical axis wind turbine, bio-inspired, sliding mesh, CFD.

1. Introduction

Wind energy harvesting has been a prominent form of renewable energy harvesting in several countries. In the high rise of energy consumption and serious pollution incurred by depleting oil and gas industry. Several countries have taken initiative in venturing into renewable energy or green energy, in order to educate the public and private agencies on the important of green energy and sustainable energy. Although wind energy is the oldest form of energy harvesting, is still considered as a developing engineering and scientific field of study. Engineers and scientist around the world are developing and designing new forms of wind turbine blade design and configuration in order to improvise the efficiency of the turbine. Meanwhile in Malaysia, wind energy harvesting is not widely embraced by the public and private sectors due to the contradicting data provided by researchers on wind speed potential [1].

Savonius wind turbine are drag driven and operates on the force applied on the blade by moving air causing the vertical shaft to rotate. Generally, drag driven wind turbine composed of two blades, where the blades are configured to face opposite to each another, therefore making the turbine an omnidirectional. Research shows that, the number of blades have an impact on the performance of the wind turbine [2]–[5]. Savonius wind turbine with two blade has higher performance efficiency than three blades [6]. Drag driven wind turbine blade shape is orientated in concave and convex surfaces [7]. The maximum power, P , extracted by wind turbine can be evaluated as expressed in Equation 1-2; where T , is torque; and ω , is angular velocity. Zhang et al. [8] stated that Savonius wind turbine is adequate for medium and mini scale in wind energy extraction. Savonius turbine holds many advantages mainly in terms of construction such as: low manufacturing cost; and less complex fabrication methodology [9].

$$K_E = \frac{1}{2} \rho v^2 \quad (1)$$

$$P = T\omega \quad (2)$$

Wind turbine rotor efficiency depends on the amount of kinetic energy extracted from the flowing air, as illustrated in Equation 3. E represents the kinetic energy of moving fluid; ρ , density of air; S_A is swept area; v is velocity of flowing fluid. The amount of energy harvested depends on the type of rotor axis configuration. Studies indicated that lift driven wind turbines are more efficient than drag driven due to its high aerodynamic performance [10]. However, due to the limitations by the laws of physics and nature, there are no wind turbine design that is able to extract 100% energy from the moving air. The maximum power coefficient, C_p , for wind turbine is 0.593 as stated in Betz law. However, the value is theoretical, thus the efficiency of wind turbine is much lower due to energy loss in shaft and gear transmission, vortex shedding, and wake rotation, as Betz law assumes constant linear velocity.

$$E = \frac{1}{2} \rho S_A v^3 \quad (3)$$

Rezaeiha et al. [11] carried out CFD analysis on 2D two bladed vertical axis wind turbine (VAWT) with moderate tip speed ratio of 4.5. The VAWT was simulated using unsteady Reynolds average Navier stokes (URANS). The author stated that in CFD simulation the domain size is the key role in accurately predicting the performance of wind turbine, where large enough domain size minimizes the effect of blockage and uncertainties in boundary condition. Three refined grids were employed to perform grid dependency study. Furthermore, refining azimuthal increment from 10.0° to 0.5° resulted in 43 % increase in power coefficient (C_p) prediction. Lam et al. [12] investigated on near and far wake on a 2D and 3D model of two blades VAWT through CFD numerical analysis. The CFD model was validated against stereoscopic particle image velocimetry (PIV) literature data. The author stated that there was no indication that detached eddy simulation (DES) performed better than transition shear stress transport (SST) in result validation comparison. Hence, the author selected transition SST for the simulation procedure. The result in 3D simulation showed that, free stream flow and strong vortices motion are two important motions in wake development. Furthermore, 2D model overestimated torque coefficient (C_t) value at tip speed ratio of 4.5.

Almohammadi et al. [13] investigated four methods of meshing; mesh refinement, General Richardson Extrapolation (GRI), Grid convergence index and fitting method to achieve a mesh independence solution for a 2D VAWT. In the CFD analysis, unsteady Reynolds average Navier stokes (URANS) was used with two turbulent models; shear stress transport (SST) and renormalized group (RNG) $k-\varepsilon$ model. The result showed that, grid convergence index may not be suitable for mesh independence solution due to its oscillation behavior in power coefficient (C_p) convergence. However, General Richardson extrapolation (GRI) provides the result that was more promising. Fitting method shows positive result in mesh independence solution. Rezaeiha et al. [14] stated that parameters such as azimuthal increment, domain size and number of revolutions have profound effect on the accuracy of a CFD simulation. The author investigated the impact of the parameters on the accuracy of simulation result by simulating a VAWT at different tip speed ratio and solidities. The result showed that, azimuthal increment is dependent on tip speed ratio. Dynamic stall happens at turbine blades and blade wake interactions at low tip speed ratio; therefore, a finer time step is required to simulate complex flow. Ferrari et al., [15] conducted study on Savonius wind turbine using Openfoam. The conducted turbulent sensitivity study with three turbulent models. It is found that Spalart Alamaris and $k-\varepsilon$ underestimated by 10% of result generated by SST $k-\omega$. Author stated that SST $k-\omega$ is a robust turbulent model in URANS modeling for 2D analysis.

Mathematical models are utilized to analyze and evaluate the performance of VAWT. There are several numerical models available such as single streamtube model (SSM), double multiple streamtube model (DMS), multiple streamtube model and vortex model, therefore an appropriate mathematical model must be used to suit the type of wind turbine since VAWT is categorized into lift and drag type. DMS and SSM are widely used to analyze aerodynamic performance of Darrieus wind turbine. Vortex model commonly prefers the use of mathematical approached to express the performance of lift type VAWT [16]. Vortex models are potential flow models, which are used to calculate velocity fields caused by the vorticity in the wake region of the blade. Blade element momentum (BEM) model are often to be used in aerodynamic performance analysis of HAWT. In order to solve Navier-Stokes Equation (NSE), the partial differential equations (PDE) in a model has to be converted into algebraic equations. The conversion of PDE to algebraic equations are classified into three groups: finite volume method (FVM); finite difference method (FDM); finite element method. FVM method or often called as box method is widely used in wind turbine simulations. The working principal of FVM method is by employing a specific control volume, where the equations are discretized using integral formulation with grid configured sets. LES models are more suitable to analyze 3D models, and DNS model are more elaborated method in analyzing flow field which consumes high computational power and not suitable for industrial application and study [17]. Solving NSE using DNS method requires high mesh resolution and supercomputer processing capabilities for numerical investigation [18]. Although research indicates that LES model is

more accurate in comparison to other models, RANS is preferred based on its popularity and computational cost. Meanwhile, DES method is a combination of RANS and LES method, where RANS is used to numerate the eddies within and near to boundary layer zone while LES for far field zone. Although the DES is widely used for the analysis of HAWT, some researchers are skeptical in the reliability and performance of DES model in accurately predicting the global aerodynamic characteristics of HAWT [19].

In accordance to literature survey, conventional drag driven wind turbine indicated low efficiency and unreliable at Malaysia wind speed. Therefore, a novel drag driven vertical axis wind turbine is being proposed for offshore regions. This paper presents the computational numerical investigation of the bio-inspired vertical axis wind turbine in 2D in order to study the credibility of the proposed design relative to proposed morphology and outline design feature. Literature review indicated that bio inspired wind turbine design has improved the efficiency of the turbine as shown in research conducted by Fish, et al. [20] and V. Cagnet [21]. In this research the proposed design was modelled using Savonius wind turbine's configuration as reference and benchmark. Therefore, design parameters and configuration of Savonius wind turbine was adapted to perform numerical study on the proposed design. Due to the limitation in computational power, a section of the proposed design at 4m height from datum is used to conduct CFD numerical study as displayed in Figure 1. This paper will conduct numerical study of the proposed design at preliminary stage in order to find the advantages and limitations of the adapted design for future design improvement and modification.

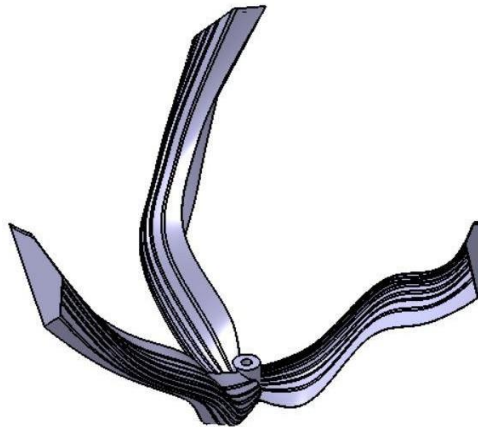


Fig. 1 - Proposed wind turbine

2. Computational methodology

2.1 Design configuration

The presented wind turbine design is inspired by three nature elements which is albatross wing, tulip flower and pitcher plant. Each design adaption plays an important role in aerodynamics of the wind turbine design. As shown in Figure 2(a), the curvature of the blade is adapted from albatross wing. The purposed of albatross wing adaptation is to provide a blade design for non-uniform pressure and drag loading in the middle section. The second adaption is tulip flower because of its concave and convex properties. Conventional Savonius wind turbine consist of concave and convex blade which plays similar role as tulip petal shape in capturing and gathering wind energy by means of drag force as displayed in Figure 2(b). The final adaptation is pitcher plant, the configuration and vane outline as shown in Figure 3(a) and 3(b). The design shape morphology consists of three novel cavity vanes at different swept angle as shown in Figure 4(a) and 4(b). Table 1 reports the dimensions of the cavity vane. Since the design are intended to be economical and to be utilized in offshore wind speed area, factors such as the amount of material required to construct the blade and the capabilities to produce torque concerned the design. The amount of material used to construct the wind turbine are less in comparison to current existing design such as Savonius, and Helical Savonius wind turbine with regards to the same aspect ratio as displayed Figure 5(a). Due to the limitations of computational power, the computational numerical study of the design is conducted in 2D. Figure 5(b) shows the geometry for CFD simulation. The proposed design was model in accordance to vertical axis wind turbine (VAWT) configuration. Therefore, design parameter of VAWT were adapted as reference to model the proposed design. Table 2 reports the geometrical parameters. The proposed morphology is an outcome of hybrid combination of the outline vertex feature points of the aforementioned nature elements. The design is modelled in CATIA via surface sweep and multi-section feature in generative shape design. More information on proposed design can be found in S.Ashwindran [22]

$$A.R = \frac{H}{D_r} \quad (4)$$

$$S_A = D_r \times H \quad (5)$$

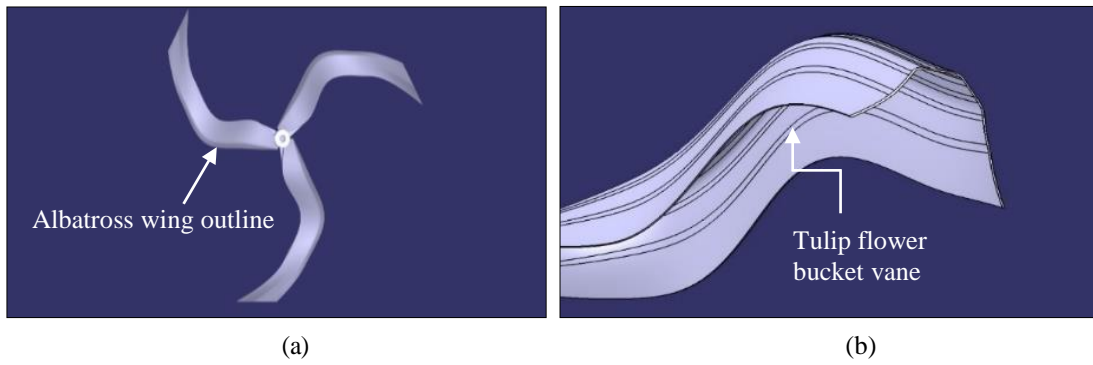


Fig 2. Blade design adaptation: (a) Albatross wing outline, (b) Tulip flower bucket vane

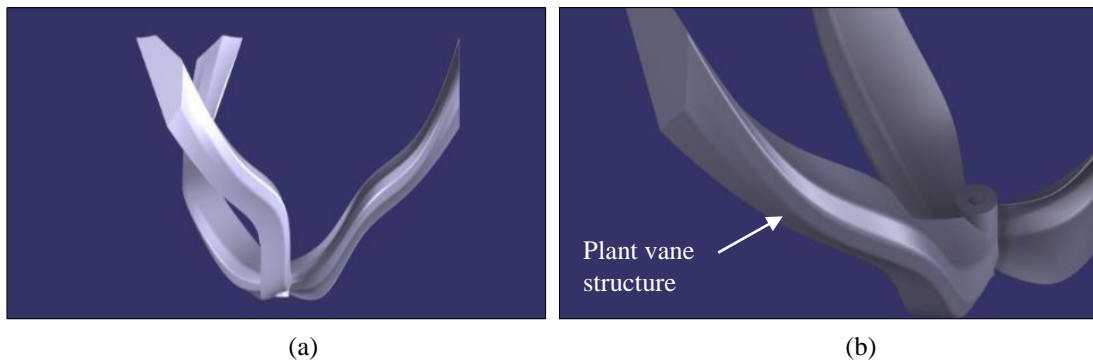


Fig 3. Pitcher plant blade design adaptation: (a) Curvature and configuration, (b) Vane structure

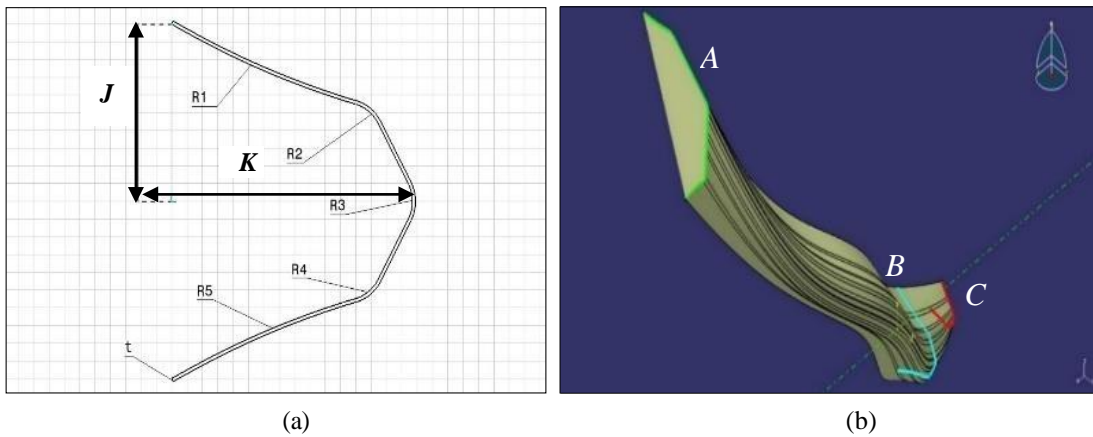


Fig 4. (a) Cavity vane profile (b) Cavity vane A, B, C with different size

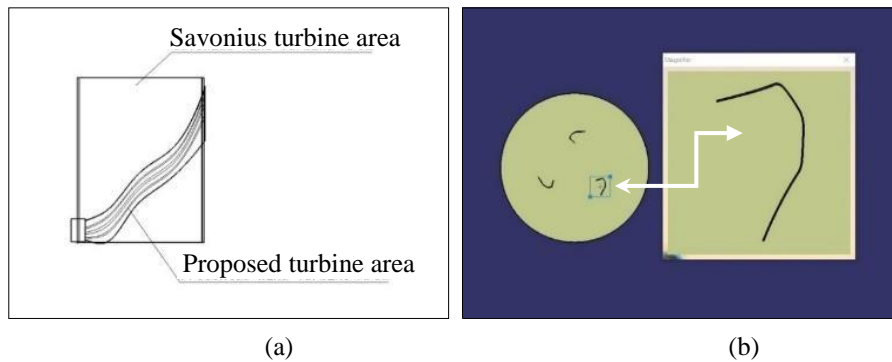


Fig 5. (a) Overlapping area comparison between Savonius and proposed design, (b) Boolean subtracted geometry for CFD simulation

2.2 Model geometry configuration

As manifested in Figure 6(a), the proposed cavity vane is constructed based on geometrical parameters. Conventional drag driven wind turbines are composed of semi-circles in concave and convex configuration. Figure 6(b) present the blade comparison under similar dimensionless aspect ratio (x/D). Although semi-circle wind turbine blade is more symmetrical in comparison to the proposed blade geometry. The purpose of the proposed geometry is to increase the height of the of blade to ensure more wind energy is capture in a converging manner. The proposed geometry is separated into two sections which is the converging section and high-pressure sections as displayed in Figure 6(a). The role of the converging section is to converge the wind flow and direct it to the following region. The high following region consist of the three arc sections as presented in Figure 6(a). The arc sections of A and C are the result of tangent lines of 60° . Arc A, B and C has a radius of $0.024m$. The arc section is intended to increase the pressure at the points A, B, and C as in contact with wind. Since the blade height of the proposed blade is higher than the conventional blade, the position of centroid of the blade will be also be higher than the conventional blade. Due to the complexity of the geometry the outline of the proposed geometry is simplified in order to obtain the estimated centroid position as shown in Figure 6(c). Based on Equation 6, the centroid of the proposed geometry is $\bar{x} \approx 0.09m$ and $\bar{y} \approx 0.064m$. Meanwhile, the centroid coordinate of semicircle is $0.042m$. Assuming the geometries as shown in Figure 6(b) is utilized to construct the wind turbine under the similar proposed design configuration. Moment of inertia of the geometries were numerated based on Equation 7. Moment of inertia describes the amount of energy gained by the rotating center for rotation at a given angular velocity [6]. The angular rotation and power coefficient of the turbine relative to the wind speed are depended on the moment of inertia [23], [24]. The moment of inertia is numerated based on Equation 7. Similar methodology in numerating moment of inertia are found in research conducted by [6]. For simplicity only moment of inertia of blades are numerated, where rotor and shaft moment of inertia is excluded. Since moment of inertia is the product of mass and radius of the elements to the axis of rotation. An arbitrary infinitesimally small element area of the geometry is used to numerate the polar moment of inertia or second moment of the semicircle element as displayed in Figure 6(d) using Equation 7. For simplicity both the geometries are assumed to have similar physical properties such as mass and thickness. Due to the complexity of the proposed shape parallel axis theorem were used to estimate the polar moment of inertia about z -axis as shown in Equation 8. Since the simplified geometry is a composite of triangle and trapezium. The geometrical properties of triangle and trapezium such as base height, length to axis of rotation are represented as C and k for simplicity. Estimated values indicated that proposed geometry has higher moment of inertia than semicircle geometry. The presented value for the proposed geometry is based on theoretical assumption which can't be accounted as obsolete since the geometry of the blade is higher asymmetrical.

$$\bar{x} = \frac{\int \tilde{x}dA}{\int dA}, \bar{y} = \frac{\int \tilde{y}dA}{\int dA} \tag{6}$$

Polar Moment of inertia of semicircle:

$$I = m \int_0^{\frac{\pi}{2}} (d \cos \alpha)^2 dm = \frac{4}{3\pi} md^2 \tag{7}$$

Polar Moment of inertia of proposed geometry:

$$I_{axis} = I_{axis'} + Ad^2 \approx \frac{c}{48} + \frac{k}{12} + Ad^2 \tag{8}$$

Table 1 Cavity vane dimension

Cavity vane (A)	Value	Cavity vane (B)	Value	Cavity vane (C)	Value
R ₁ , R ₅	0.6 m	R ₁ , R ₅	0.6m	R ₁ , R ₅	0.6m
R ₂ , R ₄	0.024m	R ₂ , R ₄	0.024m	R ₂ , R ₄	0.024m
R ₃	0.04m	R ₃	0.04m	R ₃	0.04m
K	0.08m	K	0.16m	K	0.2m
J	0.05m	J	0.1m	J	0.2m
α	25 ⁰	α	0 ⁰	α	25 ⁰
t	0.02m	t	0.02m	t	0.02m

Table 2 Geometrical parameter

Parameters	Value
Number of blade (N)	3
Height (H)	1m
Rotor diameter (D_r)	1.9m
Swept area (S_A)	19m ²
Aspect ratio ($A.R$)	0.5

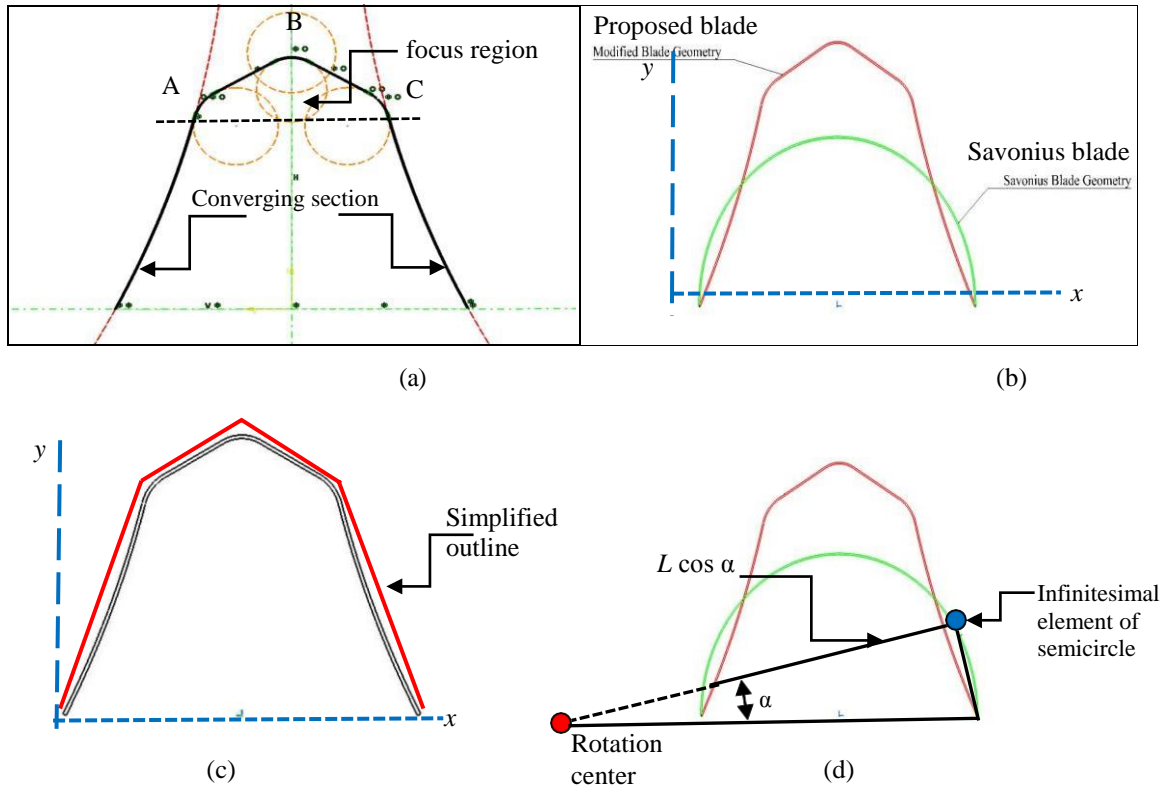


Fig 6. (a) Proposed blade geometry, (b) blade geometry comparison, (c) simplified blade geometry, (d) infinitesimal element of the geometris.

2.2 Computational configurations

The 2D proposed design is simulated using finite volume method (FVM). Therefore, a virtual wind tunnel domain was constructed as displayed in Figure 7(a). The main domain consists of static mesh with triangular mesh discretized under fine mesh densities. Previous mesh decency study indicated trivial discontinuities between fine and medium mesh, hence fine mesh is chosen for simulation. Sliding mesh configuration were used to separate the static and moving mesh. The discretized spatial mesh consists of two domains; main and rotating domain. The rotating domain is separated from the main domain by interface as shown in Figure 7(a). Non-conformal mesh was employed on the domains to ensure discontinuities in node connectivity. In order to capture the flow field properties, the blade region is mapped with 17 inflation layers with growth ratio of 1.2 as shown in Figure 7(b) and 7(c). The main domain and rotating domain are discretized with distinct face size in order to prevent mesh topological errors. Due to the complex geometry of the proposed blade, face size and mesh method were taken into careful consideration. Poor mesh configuration lead to inappropriate mesh topology and inaccurate numerated results.

In terms of boundary condition, the main domain consist of two symmetry walls, and the inlet was discretized with freestream velocity of $U_\infty=8m/s$. The outlet gauge pressure was set to zero. The blade region was set to no slip condition with motion relative to rotating domain cell zone. The simulation was conducted in pressure-based solver in 2D planar mode. *SST k- ω* turbulent transport was used to compute the flow using unsteady Reynolds averaged Navier-stokes (URANS) numerical turbulent model. Turbulent intensity and turbulent viscosity were maintained to default values. In this unsteady flow simulation, COUPLE pressure velocity coupling solver were used with Courant number set to 10. Explicit relaxation factors (ERF) was set to 0.6. The convergence criteria were set to 10^{-5} for all the flow variables. Since the simulation is conducted in 2D the height is set to 1m [25]. In order to monitor moment coefficient

reference area was set to $1.4m^2$. In order to analyze the performance of the turbine in wind power extraction, the turbine is simulated under the influence of five different tip speed ratios, which is 0.2, 0.3, 0.4, 0.6 and 0.9. The proposed turbine is simulated at constant freestream velocity at different revolution per minute (RPM) values, resulting in different tip speed ratios. Earlier conducted studies showed that $k-\epsilon$ models are not suitable for this study due to instability in numerating the flow fields. Therefore, $SST k-\omega$ is the proper model for this study in order to obtain stable numerical oscillation. Ntinis et al. [26] stated that due to the sensitivity to near wall distribution of SST its suitable for high turbulent flow study. Time-step dependency study was not conducted in order to reduce computational and numerical analysis time. Therefore, 0.01 time-step size was used in this numerical study. The turbine was analyzed under three complete revolutions $0 \leq \theta \leq 1080$. It is recommended to simulate the turbine more than two revolutions in order to obtain numerical stability and to remove initialized boundary condition properties. As for the time-step, 20 iterations per time-step was defined. Number of time-steps can be numerated by Equation 9-11.

$$\omega = 2\pi \frac{f}{60} \tag{9}$$

$$\omega = \frac{d\theta}{dt} \tag{10}$$

$$dt = \frac{2\pi}{\omega} \tag{11}$$

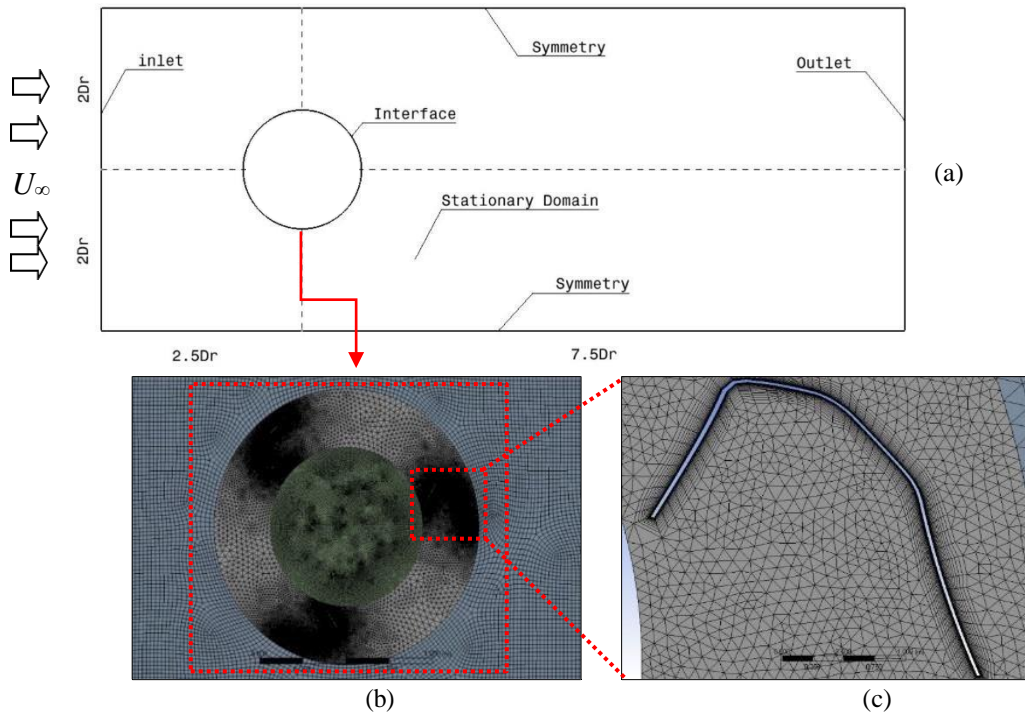


Fig 7. Domain configuration: (a) Overall configuration and dimension, (b) rotating domain, (c) inflation layer around blade region

2.3 Numerical performance parameters

The proposed wind turbine is scrutinized for three key parameters, which are moment coefficient, tip speed ratio and power coefficient. Equation 12-14 are used to numerate and study the behavior of the turbine. The efficiency of the turbine is dependent on the energy extracted by the blades from flowing wind. Therefore, the power coefficient of the proposed design under freestream velocity of $U_\infty=8m/s$ and tip speed ratio of $\lambda=0.9$ were analyzed. The simulation is conducted in a specific direction in order to study the behavior and flow response relative to the defined boundary condition.

Moment coefficient

$$C_m = \frac{M}{\frac{1}{4} \rho S_A U_\infty^2 D_t} \quad (12)$$

Tip speed ratio

$$\lambda = \frac{\omega \times \left(\frac{D_t}{2}\right)}{U_\infty} \quad (13)$$

Power coefficient

$$C_p = C_m \times TSR \quad (14)$$

3. CFD numerical result

Based on the generated moment coefficient result as shown in Figure 8, the turbine responded with positive power coefficient and stable numerical oscillation at tip speed ratio $\lambda=0.2$ and $\lambda=0.3$ which is at 20 RPM and 30 RPM respectively. However, the moment and power coefficient begin to decline and exhibit unstable behavior at $\lambda=0.4$, $\lambda=0.6$ and $\lambda=0.9$. Therefore, tip speed ratios $\lambda=0.2$, $\lambda=0.3$ and $\lambda=0.9$ were chosen for further analysis in order to study the turbine's aerodynamic behavior at respective tip speed ratios. As illustrated in Figure 7(a), the turbine at $\lambda=0.2$ generated a stable average moment coefficient value of $C_m = 0.143304$. It is observed that the numerical oscillation starts to stabilize after 100° for $\lambda=0.2$ with a constant and stable peak moment coefficient value of $C_m=0.387$. The highest moment coefficient value for $\lambda=0.2$ is indicated in the initial rotation period from $0 \leq \theta \leq 98$ with $C_m=0.572$ as displayed in Figure 8(a). Similar high moment coefficient behavior was indicated by $\lambda=0.3$ this is because the blade requires high amount of energy to initiate the rotation. Meanwhile, at $\lambda=0.3$ the turbine begins to indicate a trivial instability in moment generation at $270 \leq \theta \leq 1080$. Prior to 270° the turbine at $\lambda=0.3$ exhibited fluctuating moment coefficient with peak value of $C_m=0.353$ as displayed in Figure 8(b). Moment generation drops after 120° and presented a trivial instability in numerical oscillation with an average $C_m = 0.128$. The overall average of moment coefficient at $\lambda=0.3$ is $C_m=0.0847$. In terms of power coefficient, $\lambda=0.2$ and $\lambda=0.3$ generate $C_p = 0.029$ and $C_p=0.025$ respectively. Although, $\lambda=0.2$ and $\lambda=0.3$ generated positive power coefficient (C_p), the magnitude of C_p generated is relatively low in comparison to conventional wind turbines and not efficient in harvesting energy due to the low RPM and C_p . Based on the generated numerical result, the performance of the proposed turbine is affected by the shape of the cavity vane and aspect ratio of the design configuration. The turbine indicates positive power coefficient generation at low tip speed ratio, this is due to the low adverse pressure effect induced on the sharp edges on the blades. Therefore, reducing the magnitude of form drag caused by the cavity vane. At low tip speed ratio as the blade progresses, lesser disturbance is caused by the returning blade on the advancing blade in comparison to high tip speed ratios. Since the aspect ratio of the design configuration is not adequate to the proposed morphology, it is sensible for the turbine to exhibit unstable behavior at high tip speed ratio. The curved and wide expanding blade configuration with small volume cavity vane makes it difficult to stably collect wind energy for rotation. It requires high drag force induced by high wind speed to rotate the turbine due to dead weight and inadequate aspect ratio. Hence the proposed design configuration works at low tip speed ratios with low RPM values. However, the minimum requirement to harvest energy at low tip speed ratio using ultra-low speed permanent magnet synchronous motor is 60RPM by standards. Therefore, significant design improvement has to be done in order to increase the performance of the turbine. It is noticed that the geometry of the cavity vane, aspect ratio and configuration are the main motivating factor that restricted the performance of the turbine. Figure 8(e) presents the moment coefficient result at $\lambda=0.9$. The peak moment coefficient value is at the first revolution at an average $C_m = -0.104$. The total blade moment generated by all blades is $M = -10.75 N.m$. The generated power coefficient is $C_p = -0.094$, in which low in comparison to establish wind turbines. It is observed that during $360 < \theta < 1080$ the moment generation begins to exhibit unstable behavior consequently generating negative power coefficients.

Figure 9 present the individual drag coefficient result of the blades at $\lambda=0.2$. Blade 3 indicated high drag coefficient of $C_d=0.56$ in the initial rotation cycle at $0 < \theta < 90$. This is due to blade 3 facing in upwind direction in which the blade requires high drag force to initiate the rotation. As the angular position of blade 3 increases drag coefficient drops which is gained by blade 1. As blade 1 progresses into upwind region the drag coefficients increased significantly to value of $C_d=0.55$. This sudden rise of drag coefficient presented by blade 1 is due to form drag. Since the blade geometry is highly asymmetrical with curved and skewed shape, form drag rises along the blade region. As manifested in Figure 10, the turbine generated a stable peak drag coefficient value of $C_d=0.79$ after 270° . Meanwhile at $\lambda=0.9$ the turbine presented a highly unstable behavior. As shown in Figure 11 and Figure 12, the turbine generated an unstable numerical oscillation result in comparison to drag coefficient result at $\lambda=0.2$. At $0 < \theta < 90$ blade 2 generated the higher drag coefficient in comparison to blade 1 and 3. Since blade 2 is a returning blade, generating higher drag coefficient than the advancing blade 1 implicated the moment and power extraction. It is observed as the tip speed ratio increases

under the influence of constant wind speed, drag and pressure increases on the returning blade which consequently affect the advancing blade in initiating a clean rotation.

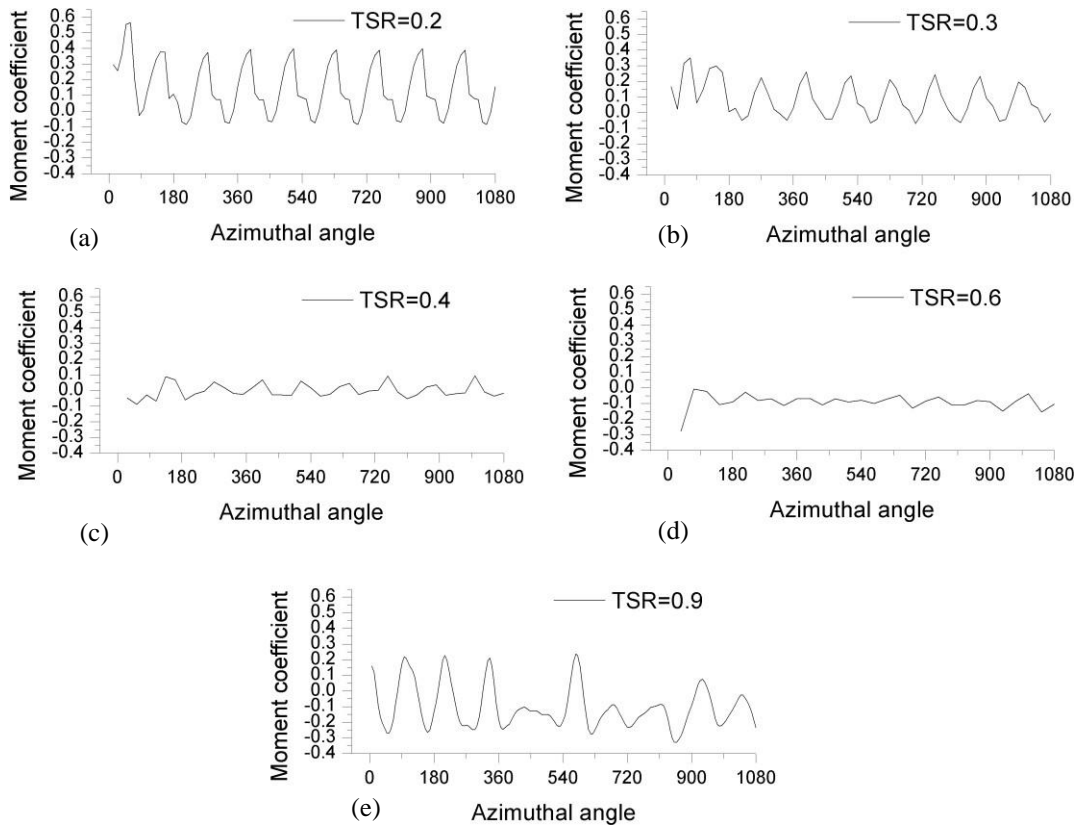


Fig. 8 - Moment coefficient of blade 1;2;3 at different tip speed ratios

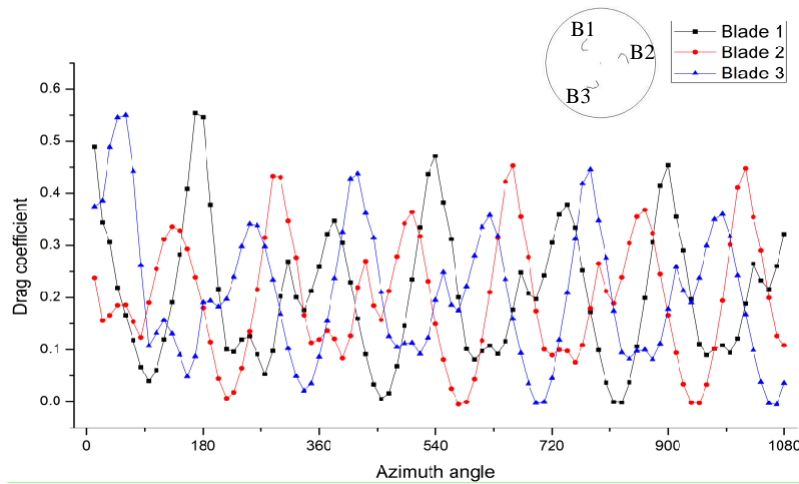


Fig. 9 - Individual blade drag coefficient at $\lambda= 0.2$

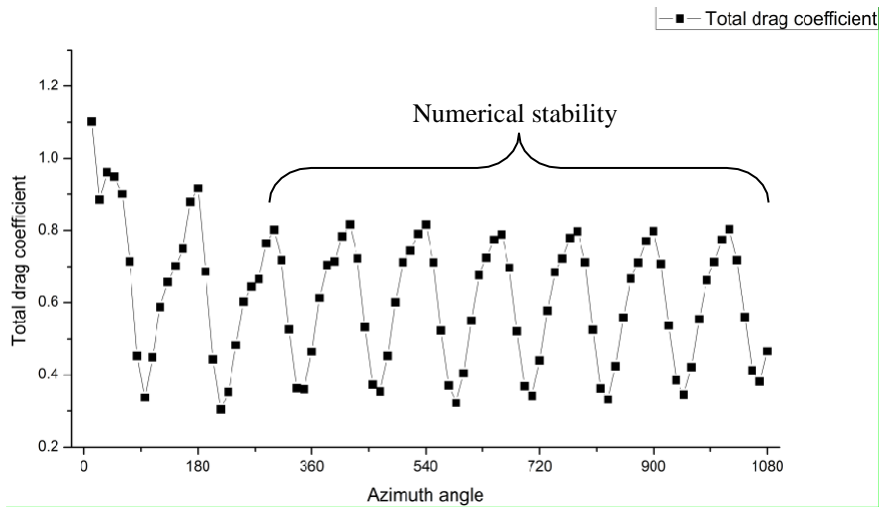


Fig 10. Total drag coefficient at $\lambda=0.2$

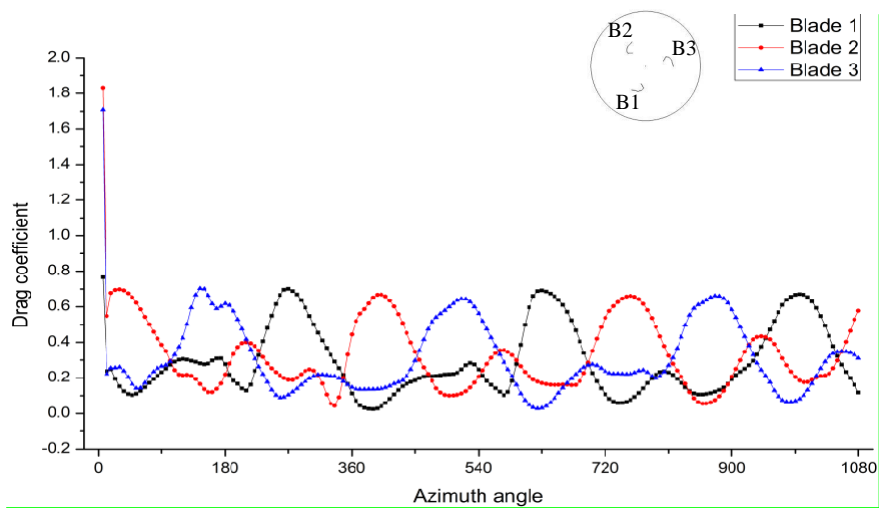


Fig 11. Individual drag coefficient at $\lambda=0.9$

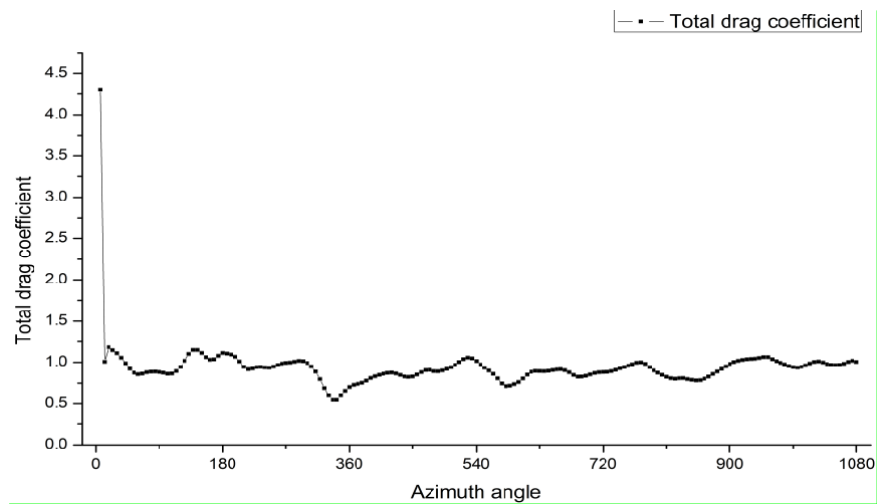


Fig. 12 - Total drag coefficient at $\lambda=0.9$

The rise in static pressure along the blade 1 region due to its geometry resulted in high form drag, therefore affecting the motion of blade 3 as displayed in Figure 13(a). Furthermore, negative pressure region is noticed behind advancing blade which is caused by wind circulation or local vortices. The rise of static pressure at the edges of the blade region leads to large reduction of moment generation, therefore making it difficult for power extraction. Negative pressure along the advancing blade region lead to significant energy loss and low power coefficient generation. As indicated in Figure 13(a), returning blade 1 experience significant pressure difference on the both regions of the blade, which generates lift in the normal direction relative to the blade. Since the turbine is configured to rotate in anti-clockwise direction advancing blade 2 in upwind region is interrupted by the lift force generated by blade 1. As manifested in Figure 13(b), low speed wake region is noticed behind the turbine region accompanied by vortex shedding. Due to the skewed and curved shaped of the blade, inconsistent strong velocity profiles are noticed along the front side of returning blade 1 and behind advancing blade 2. This inconsistent velocity streamlines resulted in unstable lift generation along the blade region which is not sufficient to assist the blades for rotation. Apart from blades geometry, the aspect ratio and swept area presented by the design also contributes to the low in performance. Since wind power extraction is a function of wind velocity, V^3 , low wind speed resulted in minimal power extraction, because of the large swept area and low aspect ratio. Due to the small cavity capturing area it is sensible for low moment generation because less energy is captured by the blade from the upwind. Furthermore, the blade operating under the influence of strong wake region which further reduce the effectiveness in power extraction. The actual power coefficient result is lower than the numerated value, $C_{p-actual} < C_{p-calculated} = -0.094$, because the presented simulation result has neglected aerodynamic and mechanical losses.

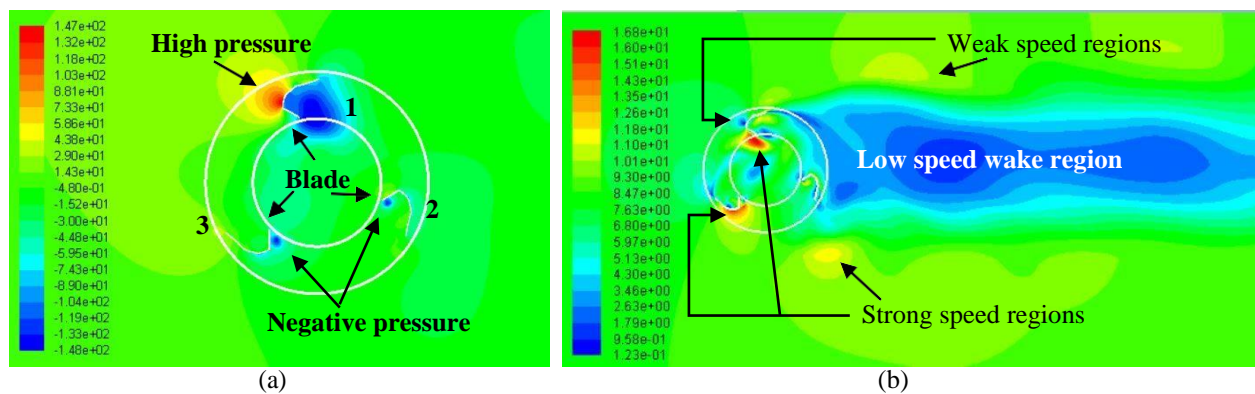


Fig. 13 - CFD contour result at $\lambda=0.9$ (a) Static pressure; (b) Velocity magnitude

In order to further study the proposed blade cavity geometry, vorticity generated along the blade region is studied. Vorticity is a pseudo vector that represents the local spinning motion of the fluid at a refer local point. Figure 14(a) and 14(b) shows the vorticity magnitude result at $\lambda=0.2$ and $\lambda=0.9$ respectively. As indicated in the Figure 14(b), the blades at $\lambda=0.9$ exhibited high chaotic wake behavior then blades at $\lambda=0.2$. local fluid spinning creating a vortex region can be observed along the advancing blade at $\lambda=0.9$ as shown in Figure 14(c) and 14(d). Since the vortex regions is located at the advancing blade, this will add resistance to the blade thus adding an opposing drag load on the advancing blade. Therefore, effecting the moment generation, this is due to the less streamline and sharp edges blade shape. At $\lambda=0.2$ no local spinning regions were indicated. This is because at $\lambda=0.2$ the turbine is revolving relatively at low *RPM*; therefore, the blade did not induce much turbulent force to induce a spinning motion or vortex in the flowing fluid. The sharp edges and expended asymmetrical geometry had created a large high turbulent trailing edge which consequently effected the following blade. The similarity can be observed at both tip speed ratios $\lambda=0.2$ and $\lambda=0.9$. The lack of streamline properties of the blade had created an unbalance load on the blades, where the blades affects one another. Furthermore, the number of blades is also the key factor, where advancing and returning blade struggles to initiate the motion due the additional weight and unbalanced force incurred by the third blade therefore making the blade difficult to create an action and reaction force. Meanwhile advancing blade at $\lambda=0.2$ did not indicate strong internal vortices as high internal turbulent vortices which can be observed on the advancing blade at $\lambda=0.9$ shown in Figure 14(c). Due to the lack of streamline internal surface, the flow exhibited a strong chaotic behavior at high tip speed ratio. Furthermore, due to the intense internal vortices it consequently decreases the pressure on the advancing blade region in which lead to negative power extraction. At $\lambda=0.2$ the turbine did not indicate any sign of tip vortices. On the contrary the turbine indicated a weak tip vortex on blade 3 as displayed in Figure 14(d). Strong tip vortices are responsible in increasing the power extraction of a turbine as stated in [27].

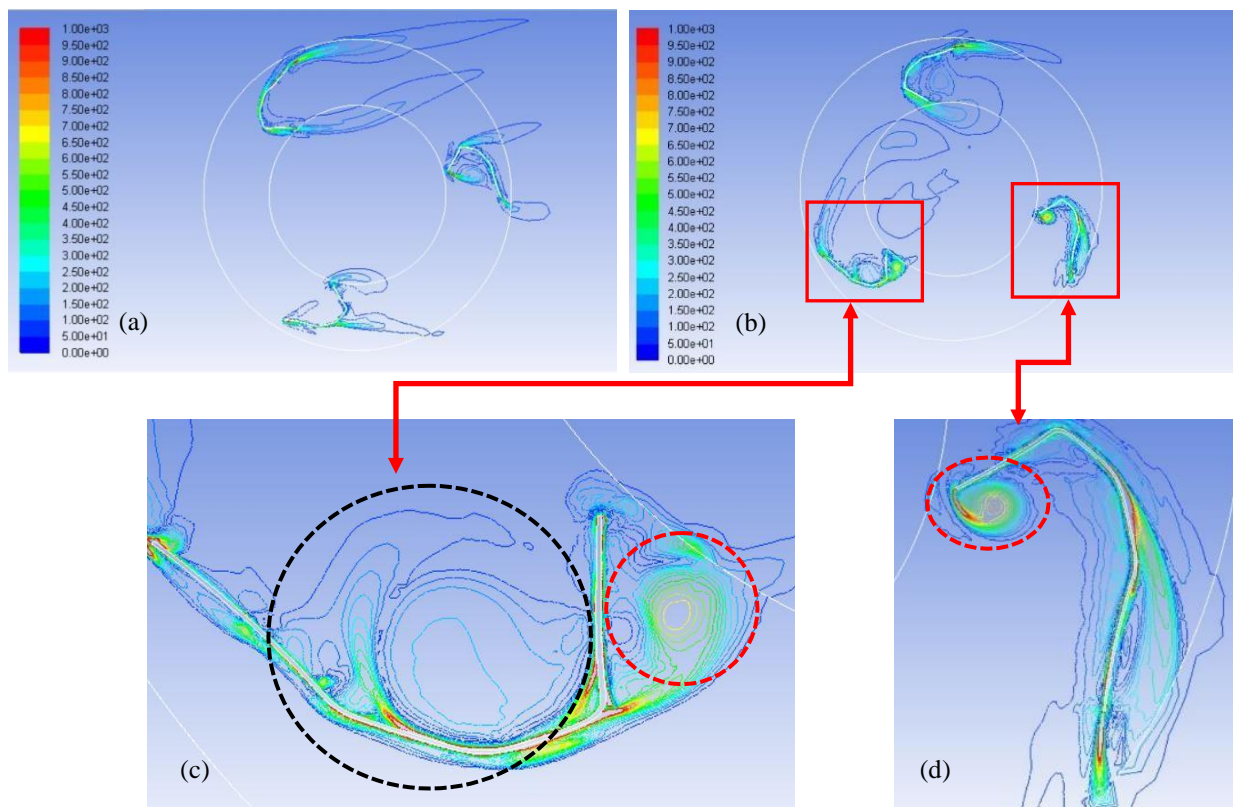


Fig. 14 - Vorticity magnitude: (a) $\lambda=0.2$; (b) $\lambda=0.9$; (c) advancing blade 1; (d) advancing blade 2

As aforementioned the proposed geometry consist of converging section and focus region. As the wind flows into the narrow section of the blade the flow area decreases therefore changing the flow field properties. The rate of change of momentum increases the fluid flow velocity and consequently decreasing the pressure. Since high pressure gradient is essential for advancing blade for angular motion. The narrowly skewed shape geometry resulted in unstable pressure distribution along the blade region. Furthermore, the geometry consists of curved section resembling convex shape. When the blade is facing in the upstream direction, the rate of change of velocity on the concave and convex regions of the blade resulted in non-uniform and unstable pressure distribution. Hence creating high pressure distribution on the outer regions of the blade. A uniform concave and convex geometry blade will result in pressure distribution as presented by [20], [22]. Figure 15 and Figure 16 shows the static pressure distribution result along the blade region at $\lambda=0.2$ and $\lambda=0.9$ respectively. As manifested in the Figure 15, at $\lambda=0.2$, the turbine exhibited a fairly stable pressure distribution along the blade region. As indicated in the Figure 15, the outer surface of blade 1 shows slightly higher-pressure distribution then the inner surface blade 3. Conversely at $\lambda=0.9$, the pressure distribution of the blades is unstable, which consequently impacted the rotation and power extraction. Blade 2 as returning blade present a higher-pressure gradient on the outer regions of the blade then advancing blade 1. Since the pressure on the returning blade is higher the advancing blade, moment generation and power extraction deteriorate. Low and high negative static pressure along the advancing blade is the result of high RPM and improper and non-streamline geometry.

Based on the result presented, the proposed geometry resulted in unstable moment generation and torque deliverance which impacted the power extraction. The lack of symmetrical and streamline properties of the blades has affected one another as in terms of rotation. Hence its sensible for the proposed turbine to indicate poor performance result in terms of power coefficient. Furthermore, the configuration properties of the turbine such as the aspect ratio is the also the root cause of poor performance. Since the blades are placed far apart for each another, the turbine experience significant energy loss. Since it's a drag driven turbine, placing the blades far apart will also further reduce interference drag. By principle, placing drag driven blade closer to each another with proper overlapping ratio will significantly increase the drag. In general, the aspect ratio and blade geometry need to be revised in order to improve the performance of the proposed wind turbine.

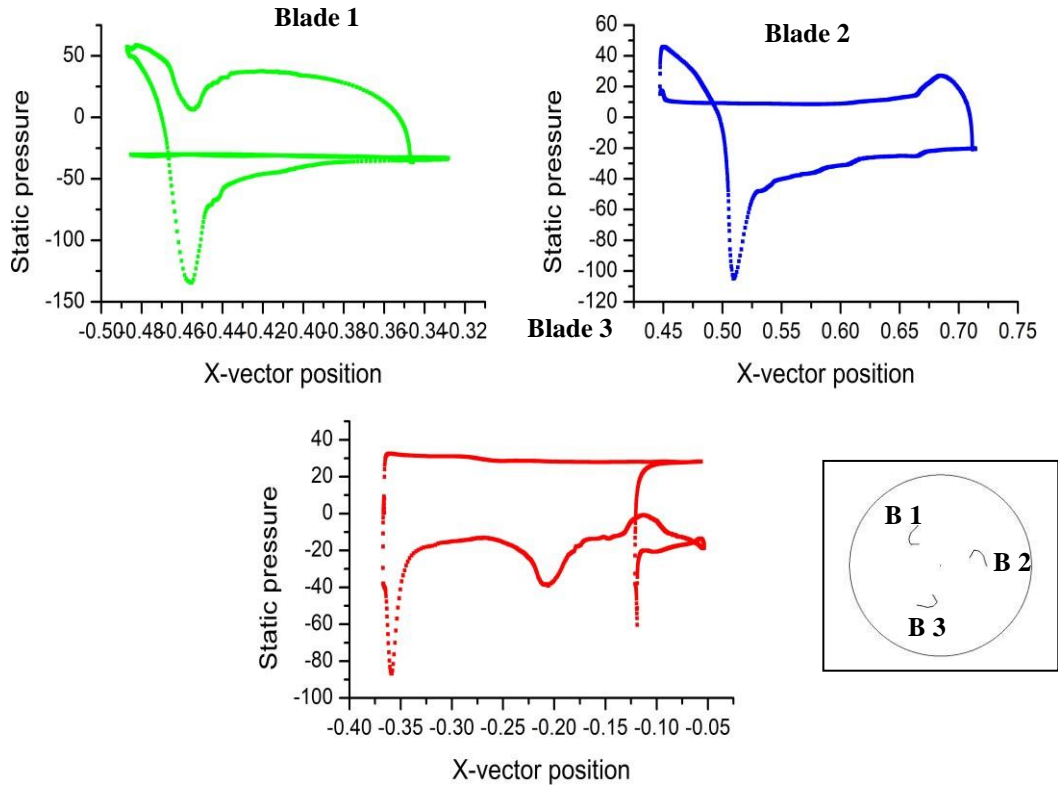


Fig 15. Static pressure distribution along the blade region by x -vector diction at $\lambda=0.2$

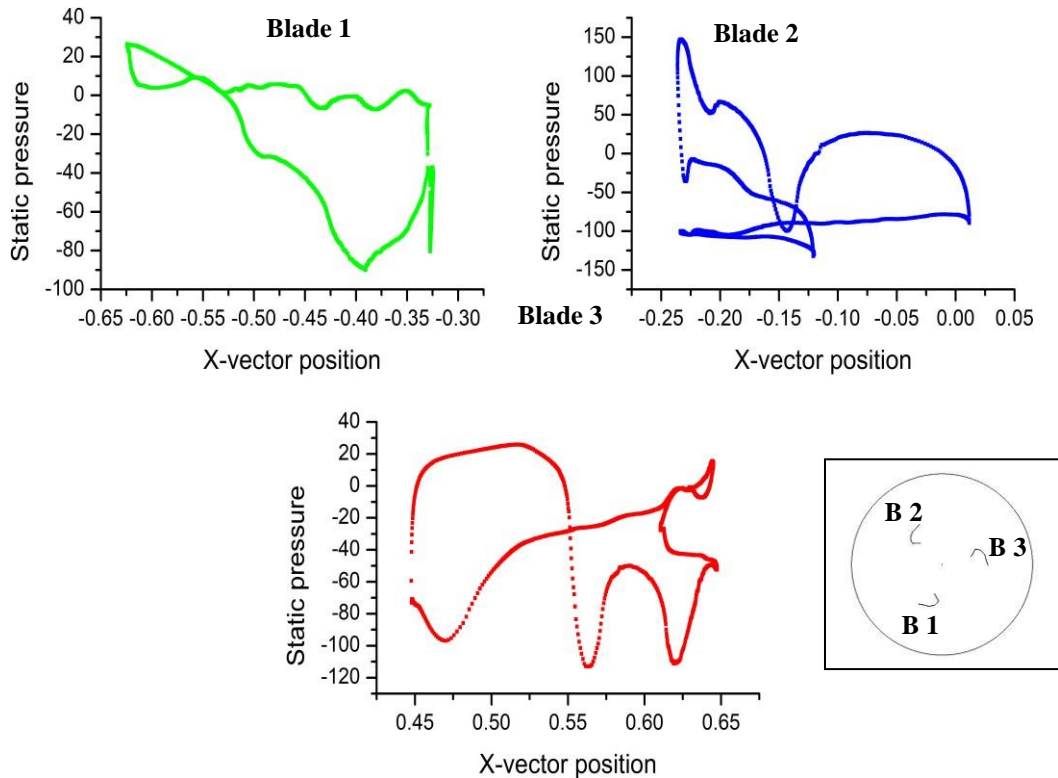


Fig. 16 - Static pressure distribution along the blade region by x -vector diction at $\lambda=0.9$

4. Conclusion

This paper presents the numerical investigation of bio inspired vertical axis wind turbine. The proposed turbine is simulated in 2D under the influence of freestream velocity of $U_{\infty}=8m/s$ at multiple tip speed ratios. Initial mesh dependency study indicated trivial dissimilarities between fine and medium mesh resolution, Therefore, fine mesh

densities were chosen for the rest of the simulations. The proposed turbine is simulated at five different low tip speed ratios. Results shows that the turbine responded well at $\lambda=0.2$ and $\lambda=0.3$ with positive power coefficient of $C_p = 0.029$ and $C_p=0.025$ respectively which is relatively low in comparison to conventional drag driven turbines. Meanwhile, tip speed ratio $\lambda=0.4$, $\lambda=0.6$ and $\lambda=0.9$ indicated high instability in moment generation and high negative power extraction. Generated result indicates negative power coefficient which has impacted the performance of the turbine. The computational study indicates that, the reason behind negative power coefficient is due to the cavity vane geometry and aspect ratio. The cavity vane experiences high adverse pressure due to its sharp cornered geometry in returning blade which consequently impacted the rotation of the advancing blade. Therefore, it is concluded that, design improvement needs to be done on the cavity vane geometry to ensure smooth transient in rotation without the blade affecting one another. Furthermore, rotor aspect ratio and swept area needed to be revised and improved to overcome the loss of energy during initial rotation due to the large swept area and dead weight. Experimental study is required in order to validate the computational numerical result and further analyzed the behavior of the proposed turbine.

Acknowledgement

This research work was conducted under Grant number RDU1901131. I would like to thank UMP for providing the computing resources.

References

- [1] L.-W. Ho, "Wind energy in Malaysia: Past, present and future," *Renew. Sustain. Energy Rev.*, vol. 53, pp. 279–295, 2016.
- [2] F. Mühle, M. Adaramola, and L. Sætran, "The effect of the number of blades on wind turbine wake - a comparison between 2-and 3-bladed rotors," *J. Phys. Conf. Ser.*, vol. 753, Oct. 2016.
- [3] M. Zheng, Y. Li, H. Teng, J. Hu, Z. Tian, and Y. Zhao, "Effect of blade number on performance of drag type vertical axis wind turbine," *Appl. Sol. Energy*, vol. 52, no. 4, pp. 315–320, Oct. 2016.
- [4] Q. Li, T. Maeda, Y. Kamada, J. Murata, K. Furukawa, and M. Yamamoto, "Effect of number of blades on aerodynamic forces on a straight-bladed Vertical Axis Wind Turbine," *Energy*, vol. 90, pp. 784–795, Oct. 2015.
- [5] P. J. Schubel and R. J. Crossley, "Wind Turbine Blade Design," *Energies*, vol. 5, no. 9, pp. 3425–3449, Sep. 2012.
- [6] M. Hadi Ali, "Experimental Comparison Study for Savonius Wind Turbine of Two & Three Blades At Low Wind Speed," *Int. J. Mod. Eng. Res. www.ijmer.com*, vol. 3, no. 5, pp. 2978–2986, 2013.
- [7] A. M. Zemamou, "Review of savonius wind turbine design and performance," *Energy Procedia*, vol. 141, pp. 383–388, 2017.
- [8] B. Zhang, B. Song, Z. Mao, W. Tian, B. Li, and B. Li, "A novel parametric modeling method and optimal design for Savonius wind turbines," *Energies*, vol. 10, no. 3, 2017.
- [9] M. Zemamou, M. Aggour, and A. Toumi, "Review of savonius wind turbine design and performance," *Energy Procedia*, vol. 141, pp. 383–388, Dec. 2017.
- [10] M. R. Castelli and E. Benini, "Comparison between Lift and Drag-Driven VAWT Concepts on Low-Wind Site AEO," vol. 5, no. 11, pp. 669–674, 2011.
- [11] A. Rezaeiha, I. Kalkman, and B. Blocken, "CFD simulation of a vertical axis wind turbine operating at a moderate tip speed ratio: Guidelines for minimum domain size and azimuthal increment," *Renew. Energy*, vol. 107, pp. 373–385, 2017.
- [12] H. F. Lam and H. Y. Peng, "Study of wake characteristics of a vertical axis wind turbine by two- and three-dimensional computational fluid dynamics simulations," *Renew. Energy*, vol. 90, pp. 386–398, 2016.
- [13] K. M. Almohammadi, D. B. Ingham, L. Ma, and M. Pourkashan, "Computational fluid dynamics (CFD) mesh independency techniques for a straight blade vertical axis wind turbine," *Energy*, vol. 58, pp. 483–493, 2013.
- [14] A. Rezaeiha, H. Montazeri, and B. Blocken, "Towards accurate CFD simulations of vertical axis wind turbines at different tip speed ratios and solidities: Guidelines for azimuthal increment, domain size and convergence," *Energy Convers. Manag.*, vol. 156, no. September 2017, pp. 301–316, 2018.
- [15] G. Ferrari, D. Federici, P. Schito, F. Inzoli, and R. Mereu, "CFD study of Savonius wind turbine: 3D model validation and parametric analysis," *Renew. Energy*, vol. 105, pp. 722–734, 2017.
- [16] J. P. Wilhelm, C. C. Panther, F. A. Pertl, and J. E. Smith, "Vortex analytical model of a circulation controlled vertical axis wind turbine," in *Proceedings of the ASME 3rd International Conference on Energy Sustainability 2009, ES2009*, 2009, vol. 2, no. January, pp. 993–1000.
- [17] R. Nobile, M. Vahdati, J. F. Barlow, and A. Mewburn-Crook, "Unsteady flow simulation of a vertical axis augmented wind turbine: A two-dimensional study," *J. Wind Eng. Ind. Aerodyn.*, vol. 125, pp. 168–179, Feb. 2014.
- [18] K. Rogowski and R. Maroński, "CFD computation of the Savonius rotor," *J. Theor. Appl. Mech.*, no. February 2015, p. 37, 2015.

- [19] H. Lei, D. Zhou, Y. Bao, Y. Li, and Z. Han, "Three-dimensional Improved Delayed Detached Eddy Simulation of a two-bladed vertical axis wind turbine," *Energy Convers. Manag.*, vol. 133, pp. 235–248, 2017.
- [20] F. E. Fish, P. W. Weber, M. M. Murray, and L. E. Howle, "The tubercles on humpback whales' flippers: Application of bio-inspired technology," in *Integrative and Comparative Biology*, 2011, vol. 51, no. 1, pp. 203–213.
- [21] V. Cagnet, S. Courrech Du Pont, I. Dobrev, F. Massouh, and B. Thiria, "Bioinspired turbine blades offer new perspectives for wind energy," *Proceedings of the Royal Society A: Mathematical, Physical and Engineering Sciences*, vol. 473, no. 2198, p. 20160726, 15-Feb-2017.
- [22] S. Ashwindran, A. A. Azizuddin, and A. N. Oumer, "Computational fluid dynamic (CFD) of vertical-axis wind turbine: mesh and time-step sensitivity study," *J. Mech. Eng. Sci.*, vol. 13, no. 3 SE-Article, Sep. 2019.
- [23] R. D. Maldonado *et al.*, "Design, simulation and construction of a Savonius wind rotor for subsidized houses in Mexico," *Energy Procedia*, vol. 57, pp. 691–697, 2014.
- [24] Y. Hara, K. Hara, and T. Hayashi, "Moment of Inertia Dependence of Vertical Axis Wind Turbines in Pulsating Winds," *Int. J. Rotating Mach.*, vol. 2012, pp. 1–12, 2012.
- [25] T. Wenlong, S. Baowei, and M. Zhaoyong, "Conceptual design and numerical simulations of a vertical axis water turbine used for underwater mooring platforms," *Int. J. Nav. Archit. Ocean Eng.*, vol. 5, no. 4, pp. 625–634, 2015.
- [26] G. K. Ntinias, X. Shen, Y. Wang, and G. Zhang, "Evaluation of CFD turbulence models for simulating external airflow around varied building roof with wind tunnel experiment," *Build. Simul.*, vol. 11, no. 1, pp. 115–123, 2018.
- [27] W. Tian, Z. Mao, B. Zhang, and Y. Li, "Shape optimization of a Savonius wind rotor with different convex and concave sides," *Renew. Energy*, vol. 117, no. October, pp. 287–299, 2018.
- [28] W. Tian, M. Zhaoyong, B. Zhang, and Y. Li, *Shape Optimization of a Savonius Wind Rotor with Different Convex and Concave Sides*, vol. 117. 2017.
- [29] X. Sun, Z. Cao, Y. Zhuang, D. Huang, and Y. Cao, "Numerical modeling and optimization of a power augmented S-type vertical axis wind turbine," *Int. J. Green Energy*, vol. 15, no. 1, pp. 13–19, 2018.